J Ther Eng, Vol. 10, No. 3, pp. 622−637, May, 2024

Journal of Thermal Engineering
Web page info: https://jten.yildiz.edu.tr
DOI: 10.14744/thermal.0000815

Research Article

Numerical investigation of fluid flow and heat transfer within multilayer wavy microchannels

Ali YAGHOOBI[1], Masoud KHARATI-KOOPAEE[1,*]

[1]*Department of Mechanical Engineering, Shiraz University of Technology, Shiraz, HHJH+MJ4, Iran*

ARTICLE INFO

Article history
Received: 12 October 2022
Revised: 13 January 2023
Accepted: 08 February 2023

Keywords:
Friction Factor; Microchannel; Nusselt Number; Thermal Performance

ABSTRACT

In this research, the fluid flow and heat transfer phenomena within wavy multilayer microchannels comprising variable wavelength and amplitude are studied in laminar flow regime. In the present work, friction factor, Nusselt number and also overall performance of the multilayer microchannel are studied at different wavelengths and amplitudes and also Reynolds numbers. Numerical findings show that an increase in the number of layers results in the increase in the friction factor and Nusselt number. It is shown that the lowest and highest friction factors correspond to the cases of increasing amplitude and increasing wavelength, respectively. It is found that the decreasing wavelength and increasing amplitude cases result in the highest Nusselt number and increasing wavelength configuration leads to the lowest Nusselt number. Results exhibit that, with increasing the Reynolds number, the friction factor depending on the number of layers may increase or decrease whereas the Nusselt number increases. Numerical results show that for one-, two- and three-layer channels, the minimum relative friction factors are 0.1%, 3.7% and 4.7%, and maximum relative Nusselt numbers are 18.2%, 45% and 45.2%, respectively. It is also shown that an increase in the number of layers and Reynolds number causes the channel overall performance to increase. The lowest overall performances is associated to the increasing wavelength structure and the highest overall performance corresponds to the increasing amplitude configuration. It is shown that for one-, two- and three-layer wavy channels, the maximum overall performances are found to be 1.16, 1.43 and 1.43, respectively.

Cite this article as: Yaghoobi A, Kharati-Koopaee M. Numerical investigation of fluid flow and heat transfer within multilayer wavy microchannels. J Ther Eng 2024;10(3):622−637.

INTRODUCTION

The subject of transferring the heat was the objective of many works in the literature such as investigation of natural convection [1], addition of nanoparticles to a base fluid [2], role of magnetic field [3] and also other fields such as aerospace applications, automobile sectors, biomedical engineering and chemical engineering areas [4]. In this context, the microchannel heat sinks have received attentions by researchers as these devices could be used as an effective means for cooling process of the electronic devices. In this field, the capacity of the channel in removing the heat and

***Corresponding author.**
*E-mail address: kharati@sutech.ac.ir

This paper was recommended for publication in revised form by Editor-in-Chief Ahmet Selim Dalkılıç

also the pumping power requirement are essential factors which must be taken into account.

Various efforts have been made in order to enhance the capacity of channels in removing the heat such as using fins [5]. One of the main techniques is to employ wavy surface for the channel wall. Mohammed et al. [6] investigated the effect of different wave amplitude on the heat transfer enhancement. They found that the heat transfer phenomenon was improved compared to the straight channel and heat transfer enhancement achievement was superior to the pressure drop penalty. Liu et al. [7] studied the effect of longitudinal and transversal-wavy structures on the thermal performance of the microchannels. Their findings revealed that the thermal performance of longitudinal wavy structure was inferior to that of straight channel while the thermal performance of transversal wavy was superior. Solehati et al. [8] performed a study to investigate mixing performance in microchannel T-junction using a wavy structure. In their study, they realized that employing wavy structure could improve the mixing quality and also performance index especially at high Reynolds numbers. Rostami and Abbassi [9] and Bazdar et al. [10] conducted a study to assess the role of wavy structure in heat transfer enhancement of microchannels using nanofluid as working fluid. They indicated that the use of wavy structure could improve the rate of heat transfer. Eltaweel et al. [11] focused on the heat transfer characteristics of wavy-tapered microchannels. They found that tapering of the wavy channel could improve the channel performance in terms of thermal resistance in comparison with un-tapered wavy channel. Gong et al. [12] performed a research to evaluate the role of dimples in wavy microchannels. In their research, they exhibited that the existence of dimples caused the boundary layer to break up and thus improvement in the channel thermal performance. Lin et al. [13] analyzed heat transfer phenomenon in wavy microchannels while the wavelength and amplitude of the wavy units were variable. They realized that wavy microchannels employing variable wavelength or amplitude wavy units could enhance the thermal behavior of the channel than those using constant wavelength and amplitude wavy units. Kumar et al. [14] compared performance of circular wavy microchannel with sinusoidal wavy microchannel. In their study, they declared that heat transfer performance of circular wavy microchannel was higher than that of sinusoidal one. Zhu et al. [15] compared performance of wavy microchannels with wavy bottom rib and side rib designs. Their results showed that the up-down wavy design led to a better performance.

In the context of fluid flow through microchannels, some studies were devoted to characterize fluid flow through straight multi-layer channels. Chong et al. [16] investigated the fluid flow within single and double layer counter flow in microchannels. Their research revealed that single and double layer counter flow microchannels have better performance in laminar flow than turbulent flow. Some studies focused on the optimization of double layer microchannels [17-20]. In these works, they found the best geometric sizes to boost the channel performance. Effat et al. [21] studied the effect of number of layers on the thermal performance of microchannels. Their results showed that employing multilayer microchannel caused the maximum base surface temperature and pressure drop to decrease. Wong and Ang [22] and Kumar et al. [23] characterized fluid flow through double layer microchannels with channel contraction. Their research indicated that tapered channel could lead to the increase in the thermal performance but caused a higher pumping power. Shen et al. [24] characterize fluid flow through the parallel- and counter-flow staggered double layer microchannel. They mentioned that the staggered configuration could lead to a better heat transfer rate and thermal performance than the conventional double layer microchannel and counter flow case had better performance than the parallel flow case. Khodabandeh et al. [25] conducted a research to evaluate the effect of sinusoidal cavities and rectangular ribs on the thermal performance of double layer microchannels. They stated that the proposed design was capable of increase in the Nusselt number but was recommended for low Reynolds number due to pressure drop penalty. Shen et al. [26] studied the effect of multiple staggered flow alternation structures in a double layer microchannel. They showed that the staggered flow alteration structure had a favorable effect on the thermal behavior with a minor increase in the pressure drop. In the other work by Shen et al. [27], the effect of staggered alteration location was studied. This work exhibited that the change in the location of staggered alteration had a favorable effect on the thermal performance while an insignificant increase in the pressure loss was observed.

Some researches were devoted to analyze fluid flow through wavy multilayer microchannels. Xie et al. [28] assessed thermal performance of single- and double-layer wavy microchannels. Their study declared that for a same flow rate, the double-layer caused lower pressure losses and overall thermal resistance than the single-layer microchannel. In another study by Xie et al. [29], the flow through parallel and counter flow double layer wavy microchannels was compared. In this study, it was found that at large flow rate, the counter-flow double-layer wavy microchannel had a good performance while for a slightly larger flow rate, the parallel configuration resulted in a better behavior. Shen et al. [30] performed a research to examine convective heat transfer of counter-flow in staggered wavy double layer microchannels. They found that in these microchannels, the ones with opposite amplitude could enhance the heat transfer rate. Wang et al. [31] carried out a research to study fluid flow and heat transfer phenomena through a new design of a double layer microchannel with combination of wavy structure and porous vertical ribs. They found that the proposed design had a good cooling performance over a wide range of pumping power.

Referring to the work mentioned above, one could see that the fluid flow and heat transfer phenomena within the wavy multilayer microchannels with variable wavelength

and amplitude has not been investigated yet. In the present work, the role of both increase in the number of channel layer as well as the different wavy patterns with variable wavelength and amplitude on the channel walls on the friction factor, Nusselt number and also overall performance of the microchannels are characterized. In the present research, laminar flow is concerned and results are obtained at different Reynolds number.

PROBLEM DESCRIPTION

In the research undertaken, the fluid flow and heat transfer phenomena through one-, two- and three layer channels are investigated. The side walls of the channels are wavy and the channel top and down walls are flat. In this work, five different wavelengths and amplitudes are considered for the side walls. The first wavy channel, which is named as the base channel, has a constant amplitude and wavelength of A = 30 μm and λ=2000 μm, respectively. For the base channel, the wall profile is obtained using the following expression:

$$y = A \sin\left(\frac{2\pi x}{\lambda}\right) \quad (1)$$

where A and λ are amplitude and wavelength, respectively, and x denotes the channel length.

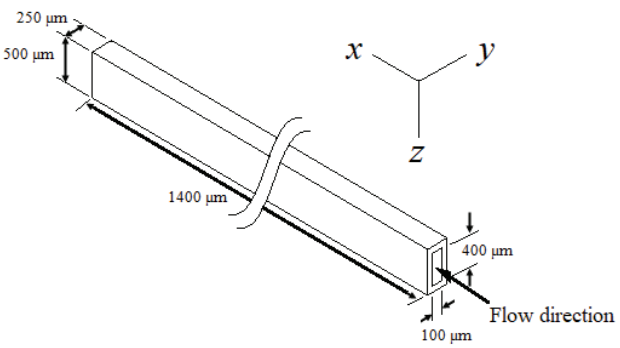

Figure 1. The one-layer base microchannel.

Figure 1 represents the single base microchannel along with geometrical parameters as well as the direction of flow entering the channel. The single microchannels are known as one-layer microchannels.

The four other wavy microchannels are obtained by varying the amplitude and wavelength of the base channel. For the two wavy channels, the amplitude is kept constant to that of the base channel (i.e., A=30 μm) and wavelength decreases and increases along the channel in such away that the difference between wave length of the two adjacent waves is $\Delta\lambda$=300 μm. For the two other wavy channels, the wavelength is fixed to that

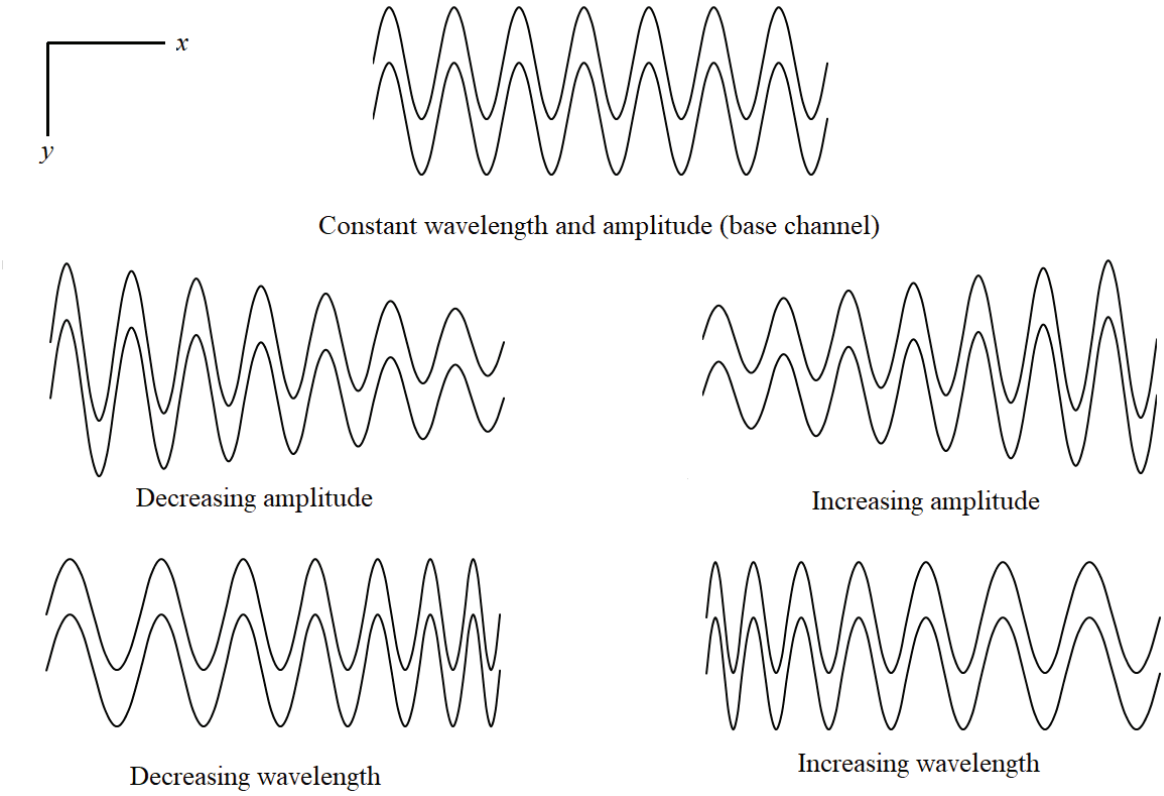

Figure 2. Inner wall profiles for the wavy microchannels on the x-y cross section at the distance of 250 μm from the channel bottom. Channels are presented with 50 magnification in y-direction.

of the base channel (i.e., λ=2000 μm) and amplitude decreases and increases such that the difference between amplitude of the two adjacent waves is ΔA=4 μm. In the present work, seven wave units are considered for numerical calculation and so, the lengths of wavy microchannels would be 14000 μm. Figure 2 depicts the inner wall profiles for the considered wavy microchannels on the *x-y* cross section at the distance of 250 μm from the channel bottom.

The multilayer microchannel is obtained by placing the same single microchannels on each other. In this work, two- and three-layer microchannels are considered to study. The considered microchannels are subjected to a constant heat flux at the bottom. Figure 3 represents front views for the one-, two- and three-layer microchannels along with geometrical parameters and also the heated wall of the microchannels.

In this study, conjugate heat transfer is concerned. Working fluid is water and material of solid wall is silicon. Fluid and channel wall properties, except fluid viscosity, are kept constant to those in the inlet temperate (i.e., T_{in}=300 K). Table 1 represents fluid and channel wall properties at the fluid inlet temperature.

Since water viscosity is more influenced by temperature than other properties, the water viscosity at fluid mean temperature is used in numerical calculation. At first, numerical

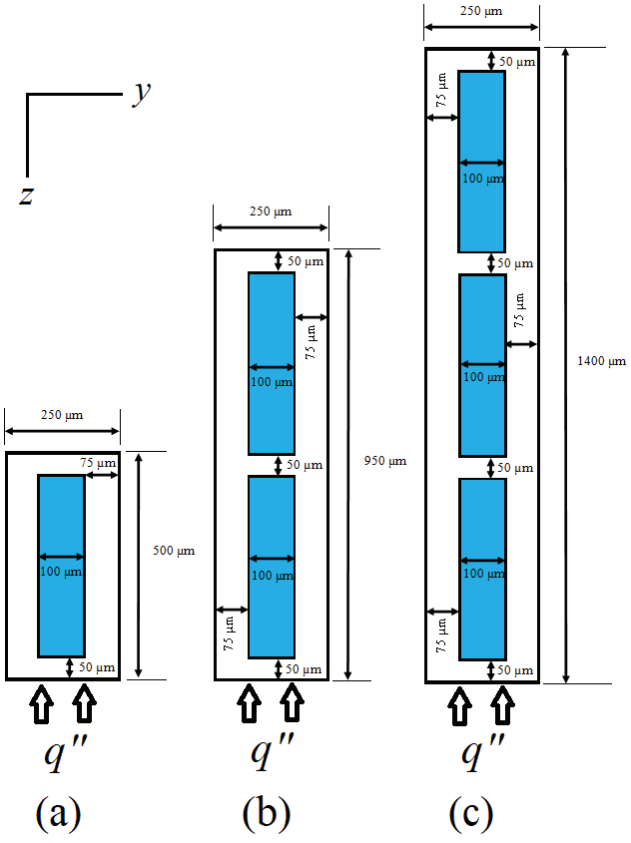

Figure 3. Front views for the (a) one-, (b) two- and (c) three-layer microchannels.

Table 1. Fluid and channel wall properties

Substance	Density, ρ (kg/m^3)	Thermal conductivity, k (W/mk)	Specific heat, c_p (J/kgK)
Water	998	0.6	4182
Silicon	2329	148	710

calculation is performed using water viscosity at the inlet fluid temperature. Then, mass average fluid temperature within the channel is computed and water viscosity at the average fluid temperature is used for numerical recalculation. Repeating this procedure, one could obtain flow field within the channel accounting temperature dependency of water viscosity. In the present work, a constant heat flux of q''=1000 kw/m^2 is applied at the bottom of the microchannels (see figure 3). To examine fluid flow and heat transfer phenomena within the considered channels, friction factor (f), Nusselt number (Nu) and overall performance of the microchannels (φ) are computed. Friction factor and Nusselt number are defined as the followings:

$$f = \frac{\frac{dp}{dx} D_h}{\frac{1}{2}\rho U^2} \tag{2}$$

$$\mathrm{Nu} = \frac{h_m D_h}{k_f} \tag{3}$$

In equation (2), dp/dx stands for pressure drop through the channel and D_h, ρ and U represent channel hydraulic diameter, fluid density and velocity, respectively. In equation (3), hydraulic diameter is defined as $D_h = 4S/P_w$, where S and P_w are cross sectional area and wetter perimeter of the channel. In equation (3), h_m also denotes average heat transfer coefficient within the channel and k_f is thermal conductivity of the fluid. For multilayer channels, the average values of friction factors and Nusselt numbers of the layers has been considered as the overall friction factor and Nusselt number of the microchannel. Heat transfer coefficient is obtained from the following:

$$h_m = \frac{q''}{(T_w - T_m)} \tag{4}$$

where T_w is average wall temperature and T_m is the mass average of the fluid temperature within the channel. Overall performance of the channel is obtained via the following relation [32]:

$$\varphi = \frac{\frac{\mathrm{Nu}}{\mathrm{Nu}_0}}{\left(\frac{f}{f_0}\right)^{\frac{1}{3}}} \tag{5}$$

In equation (5), f_0 and Nu_0 are friction factor and Nusselt number of the one-layer straight channel, respectively. Reynolds number is also defined as $R_e=\rho UD_h/\mu$, where μ is fluid viscosity at the fluid inlet temperature. For better understanding of fluid flow and heat transfer phenomena within the microcahnnels, results are obtained at Reynolds numbers of R_e=300 to 1050. This flow Reynolds number range is lower than the critical Reynolds number of $R_{e_{cr}} \approx$ 2300 and so the assumption of laminar flow is appropriate.

NUMERICAL PROCEDURE

In the current research, an incompressible flow through the channels is considered. Consequently, for the fluid flow, governing equations would be the incompressible form of the continuity, momentum and energy equations as the followings:

$$\frac{\partial u_i}{\partial x_i} = 0 \tag{6}$$

$$\rho_f \frac{\partial (u_i u_j)}{\partial x_i} = \mu_f \frac{\partial}{\partial x_i}\left(\frac{\partial u_j}{\partial x_i}\right) - \frac{\partial p}{\partial x_j} \tag{7}$$

$$\frac{\partial (u_i T)}{\partial x_i} = \frac{k_f}{\rho_f C_{p,f}} \frac{\partial}{\partial x_i}\left(\frac{\partial T}{\partial x_i}\right) \tag{8}$$

Governing equation within the channel wall is heat conduction equation and is of the following form:

$$k_s \frac{\partial}{\partial x_i}\left(\frac{\partial T}{\partial x_i}\right) = 0 \tag{9}$$

In equations (6) to (9), u_i and p are denoted for the fluid velocity components and pressure, respectively, and T represents temperature. In these equations, the subscripts f and s indicate fluid and solid properties, respectively.

Based on the considered Reynolds numbers, velocity is computed and sets for the fluid entering the channel. Pressure outlet is also set for the channel outlet. As mentioned earlier, it is assumed that the fluid with constant temperature of T_{in}=300 K enters the channel and a constant heat flux of q''=1000 kw/m^2 is imposed on the channel lower wall. Other channel walls are considered to be adiabatic. No slip boundary condition is also considered for the channel inner walls.

In this research, the generation of grid and numerical computation are performed using the commercial flow solver software, ANSYS FLUENT 16.2. In the current numerical model, the second order upwind scheme is used for discretization of momentum and energy equations and SIMPLE algorithm is utilized for the pressure-velocity coupling. The convergence criterion is based on the residuals and iteration is stopped as residuals reach less than about 10^{-8}.

Grid Study and Validation

A comprehensive grid study is performed to obtain grid independent results. To do this, for each channel, four grid levels are considered and at Reynolds number of R_e=900, friction factor and Nusselt number obtained from the considered grid levels are compared. Grid independent study reveals that for the wavy and straight channels, the grids with around 600,000 (40×750×20), 1,150,000 (77×750×20) and 1,700,000 (112×750×20) computational cells have adequate resolution for the one-, two- and three-layer channels, respectively, and maximum errors for the friction factor and

Table 2. Friction factor and Nusselt number for one-layer channel at different gird levels

Number of computational cells	Increasing wavelength		Decreasing wavelength		Increasing amplitude		Decreasing amplitude	
	f	Nu	*f*	Nu	*f*	Nu	*f*	Nu
37,500	5.4	13.8	1.9	13.3	1.6	13.6	3.9	14.5
150,000	6.4	14.6	2.3	15.3	1.9	15.3	4.7	15.1
600,000	7.1	14.7	2.6	16.1	2.1	15.9	5.3	15.5
2,400,000	7.2	14.7	2.7	16.1	2.1	16.0	5.4	15.5

Table 3. Friction factor and Nusselt number for two-layer channel at different gird levels

Number of computational cells	Increasing wavelength		Decreasing wavelength		Increasing amplitude		Decreasing amplitude	
	f	Nu	*f*	Nu	*f*	Nu	*f*	Nu
71,000	7.2	41.3	3.4	38.4	3.1	38.6	5.4	42.1
285,000	8.6	43.3	4.1	42.1	3.7	43.0	6.4	43.7
1,150,000	9.5	43.5	4.6	44.8	4.1	44.5	7.2	44.3
4,600,000	9.7	43.5	4.6	44.9	4.2	44.6	7.3	44.4

Table 4. Friction factor and Nusselt number for three-layer channel at different gird levels

Number of computational cells	Increasing wavelength		Decreasing wavelength		Increasing amplitude		Decreasing amplitude	
	f	Nu	*f*	Nu	*f*	Nu	*f*	Nu
105,000	7.1	40.4	3.9	39.3	3.5	40.1	5.2	42.5
420,000	42.9	8.5	4.7	43.4	4.2	43.3	6.6	43.9
1,700,000	43.8	9.5	5.2	45.2	4.7	45.0	7.3	44.5
6,800,000	43.8	9.6	5.3	45.2	4.8	45.0	7.5	44.6

Nusselt number are 2.2% and 0.5%, respectively. For more illustration, tables 2 to 4 show friction factor and Nusselt number for one-, two- and three-layer microchannel at different grid resolutions for the wavy channel in which the wavelength and amplitude vary along the channel.

For more illustration concerning the topology of the used grids, figure 4 depicts the grid associated to the base channel for the one-layer microchannel. The dark and white regions represent the solid and fluid portions of the computational domain.

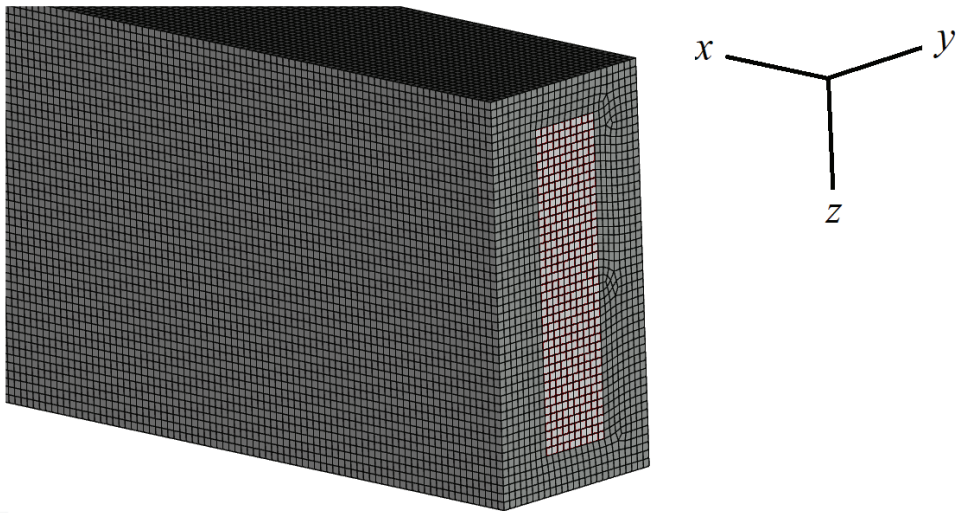

Figure 4. The grid used for numerical calculations for one-layer microchannel.

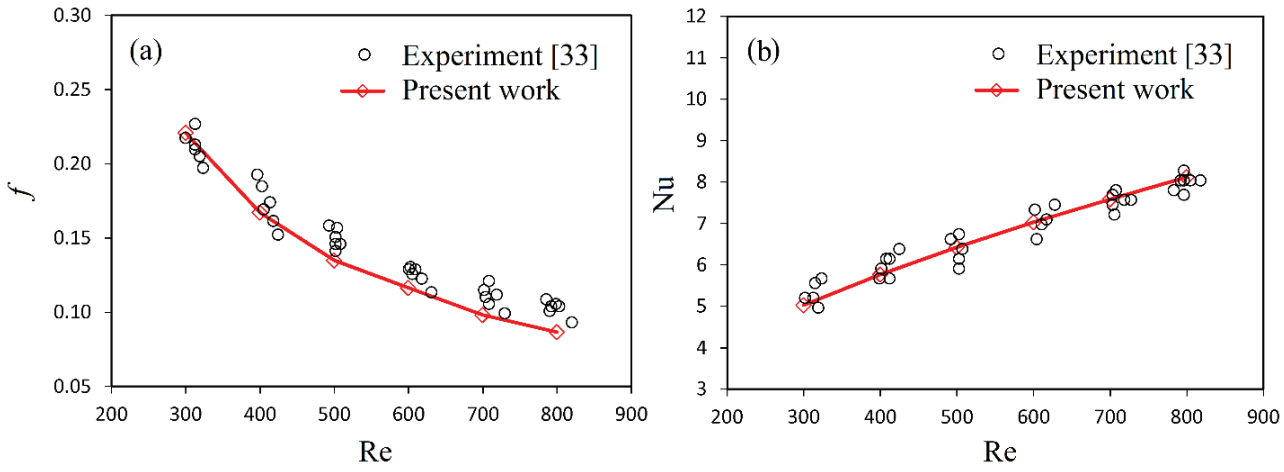

Figure 5. Friction factor (a) and Nusselt number (b) associated to the present work and experiment for the straight channel.

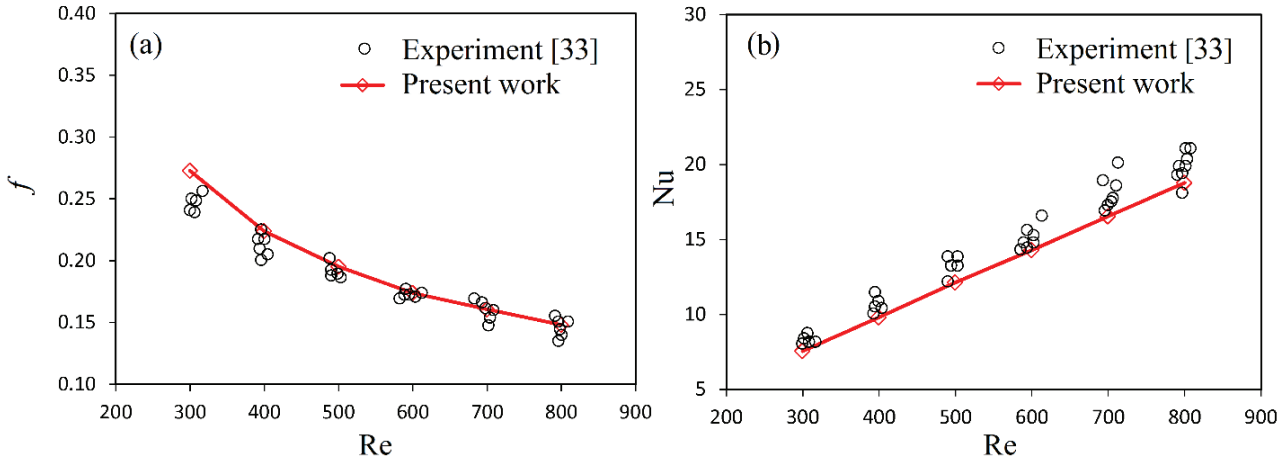

Figure 6. Friction factor (a) and Nusselt number (b) associated to the present work and experiment for the wavy channel.

The appropriateness of grids in Reynolds number of R_e=900 ensures the adequacy of the considered grids for numerical calculation at other considered Reynolds numbers.

To validate the used numerical model, friction factor and Nusselt number obtained from the present work are compared with those of experimental work of Sui et al. [33]. In the work of Sui et al. [33], the one-layer straight and wavy channel with amplitude and wavelength of 139 μm and 2500 μm, respectively, were studied. In experiment, channel wall was made of copper and a constant heat flux of q''=500 kw/m^2 was applied on the channel lower wall. Figures 5 and 6 compare friction factor and Nusselt number.

Exploring figures 5 and 6 indicates that the numerical model used for numerical calculation has adequate accuracy in prediction of friction factor and Nusselt number for the flow through the considered microchannels.

RESULTS AND DISCUSSION

For better illustration regarding the effects of employing different wavy walls for the channels or the increase in the number of channel layers, the values of friction factor and Nusselt number relative to those of the one-layer straight channel (i.e., $(f\text{-}f_0)/f_0\times100$ and $(\text{Nu-Nu}_0)/\text{Nu}_0\times100$, where f and Nu are friction factor and Nusselt number of the considered channel, respectively, and f_0 and Nu_0 denote friction factor and Nusselt number of one-layer straight channel at the same Reynolds number, respectively) are presented.

Effect on Friction Factor

Figures 7 represents variation of relative friction factor for the one-, two- and three-layer microchannels for the straight and wavy channels at different Reynolds numbers. This figure shows that for one-, two- and three-layer channels, as expected, the wavy channels result in a higher friction factor than the straight channel.

Figure 7 shows that the relative friction factor increases as the channel layers increase. To illustrate this, temperature contour at the distance of 12000 μm from the channel inlet for one-, two- and three-layer channel at Reynolds number of R_e=600 is depicted in figure 8. This figure is provided for the base channel. Exploring figure 8 shows that as the number of channel layer increases, the heat absorbed by the channel is divided between the channel layers and so a lower temperature rise is achieved for the fluid. Thus, as the water viscosity increases with decreasing the fluid temperature, one could conclude that an increase in the channel layer leads to a higher fluid viscosity and so higher pressure loss and friction factor.

Figure 7 reveals that for one-, two- and three-layer channels, the lowest and highest relative friction factors of the wavy channels correspond to the cases of increasing amplitude and increasing wavelength, respectively. Numerical findings show that for one-, two- and three-layer channels, the minimum relative friction factors are 0.1%, 3.7% and 4.7%, respectively. Figure 7 indicates that for one-, two- and three-layer channels, the relative friction factor increases as the channel configuration changes from decreasing wavelength to constant wavelength and amplitude, and finally to decreasing amplitude. Exploring numerical findings show that the change in the fluid viscosity governs the change in the friction factor. The fluid viscosity decreases as the fluid absorbs heat. Consequently, the more the fluid temperature increases, the lower the friction factor would be. To examine how the fluid temperature rises within the considered channels, the increase percentages in the mass averages of the fluid temperature relative to fluid inlet temperature for the one-layer channels at the distance of 12000 μm from the channel inlet at Reynolds number of R_e=600 is shown in figure 9. Referring to this figure, one could see that the increase percentage in the fluid temperature is the highest for the increasing amplitude cases and is the lowest for the increasing wavelength cases. This figure also indicates that

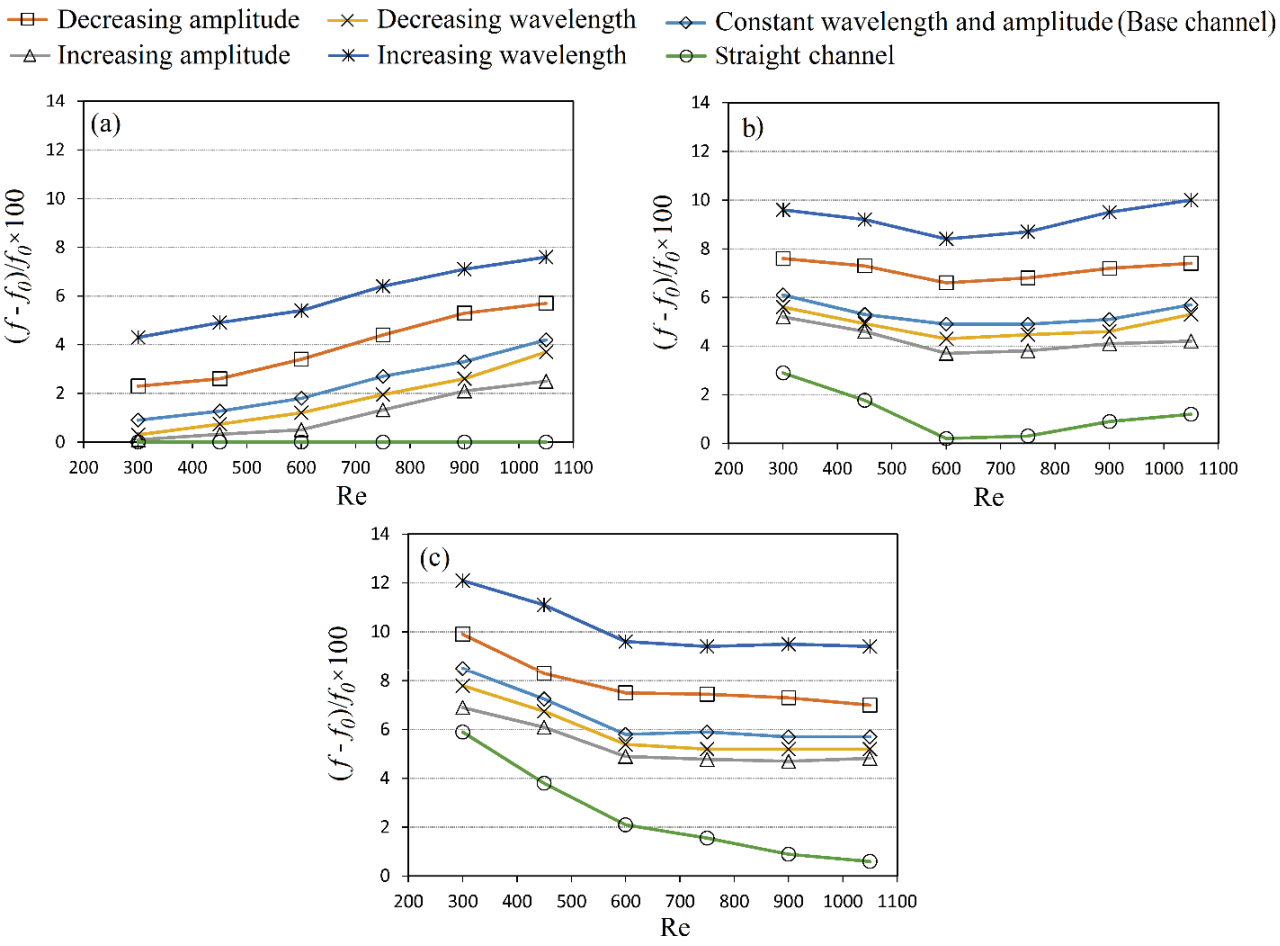

Figure 7. Variation of relative friction factor for (a) one-, (b) two- and (c) three-layer microchannels for the straight and wavy channels at different Reynolds numbers.

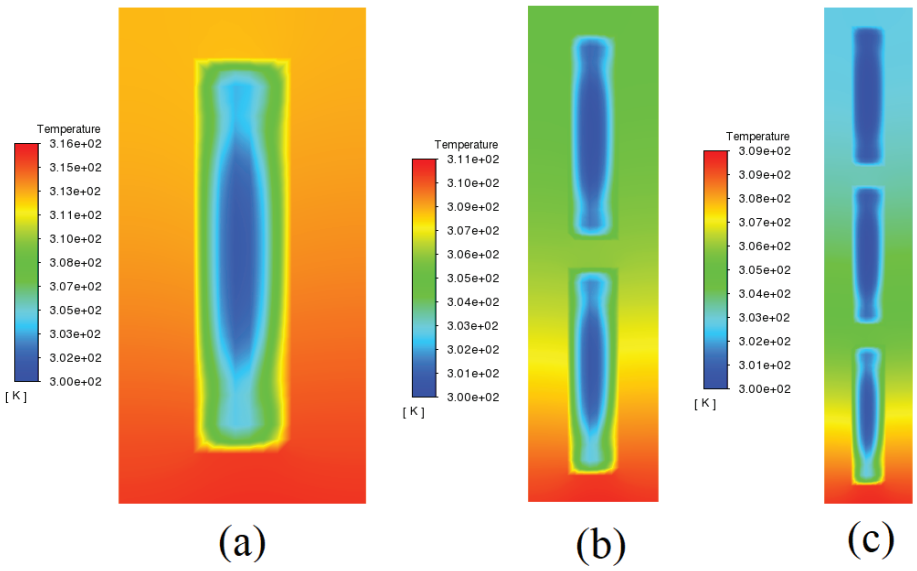

Figure 8. Temperature contour for the base channel at the distance of 12000 μm from the channel inlet for (a) one-, (b) two- and (c) three-layer base channel at Reynolds number of R_e=600.

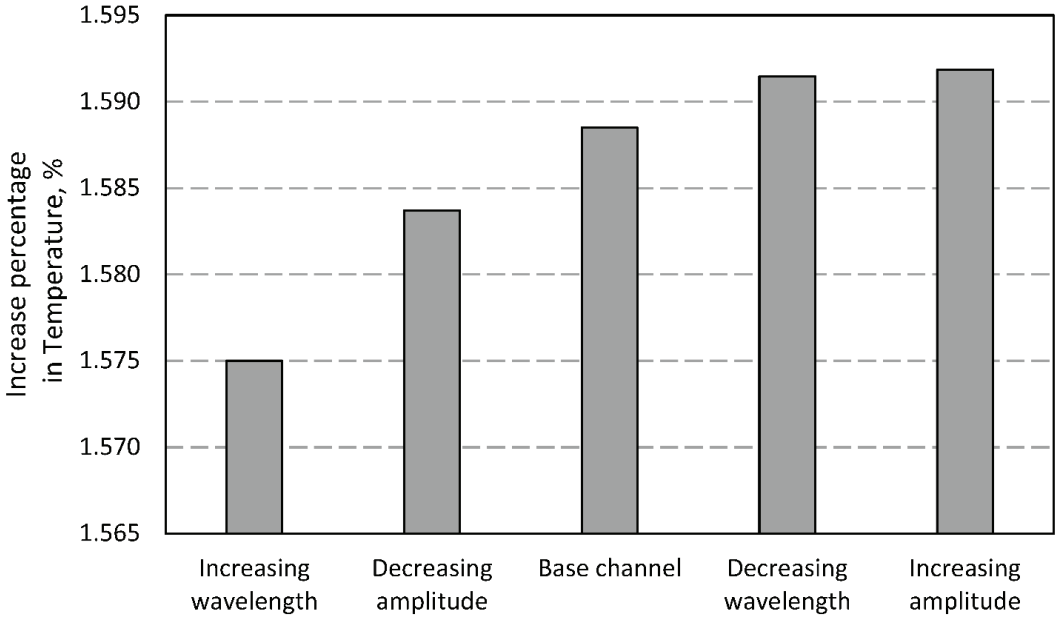

Figure 9. Increase percentages in the mass averages of the fluid temperature relative to fluid inlet temperature for the one-layer channels at the distance of 12000 μm from the channel inlet at Reynolds number of R_e=600.

the increase percentage in the fluid temperature diminishes as the channel structure changes from decreasing wavelength to constant wavelength and amplitude (base case), and then to decreasing amplitude.

Figure 7(a) reveals that for one-layer channel, an increase in Reynolds number for the wavy channel causes the relative friction factor to increase. As expected, the wavy channel results in a higher pressure loss than the straight channel as Reynolds number increases. Although the wavy channels absorb more heat than the straight channels, however, as Reynolds number increases, the effect of decrease in the fluid viscosity (due to heat absorption by the fluid) in decreasing the pressure loss is inferior to the impact of increase in the Reynolds number in increasing the pressure loss. Consequently, the relative friction factor of one-layer channel increases with increasing the Reynolds number.

Exploring figure 7(b) indicates that for the two-layer channel, the relative friction factor decreases as the Reynolds number increases from R_e=300 to R_e=600. As mentioned earlier, the two-layer channel causes higher pressure loss than the one-layer channel due to higher fluid viscosity. With increasing the Reynolds number from R_e=300 to R_e=1050, the fluid absorbs more heat which results in a lower fluid viscosity. In this range of Reynolds number, the effect of decrease in the pressure loss due to decrease in the fluid viscosity is superior to the effect of increase in the pressure loss due to increase in the Reynolds number. Thus, as the Reynolds number increases from R_e=300 to R_e=600, a lower friction factor compared to that of the one-layer straight channel could be obtained. Figure 7(b) shows that as the Reynolds number increases from R_e=600 to R_e=1050, the relative friction factor increases. Although the heat absorption capability of the fluid increases as the Reynolds number increases from R_e=600 to R_e=1050 (which leads to a lower fluid viscosity), however, the effect of decrease in the fluid viscosity in decreasing the pressure loss is not significant. Thus, the relative friction factor increases as the Reynolds number varies from R_e=600 to R_e=1050.

Figure 7(c) reveals that for the three-layer channel, an increase in Reynolds number causes the relative friction factor to decrease. As explained earlier, the three-layer channel leads to the highest pressure loss than the one- and two-layer channels due to lowest temperature rise and so higher viscosity for the fluid. As the Reynolds number increases from R_e=300 to R_e=1050, the impact of decease in the pressure loss due to decrease in the fluid viscosity is superior to the effect of increase in the pressure loss due to increase in the Reynolds number. Accordingly, for the three-layer microchannel, an increase in the Reynolds number in the considered range of Reynolds numbers causes the relative friction factor to decreases.

Effect on Nusselt Number

Figures 10 represents variations of relative Nusselt number for the one-, two- and three-layer microchannels for the straight and wavy channels at different considered Reynolds numbers. As presented in this figure, the one-, two- and three-layer wavy channels lead to a higher value for the Nusselt number than the one-layer straight channel.

Figure 10 shows that for the wavy channels, the relative Nusselt number increases as the channel layer increases from one to two. As this figure exhibits, the increase in the channel layer from two to three also causes the relative Nusselt number to increase but the increase in relative Nusselt number as

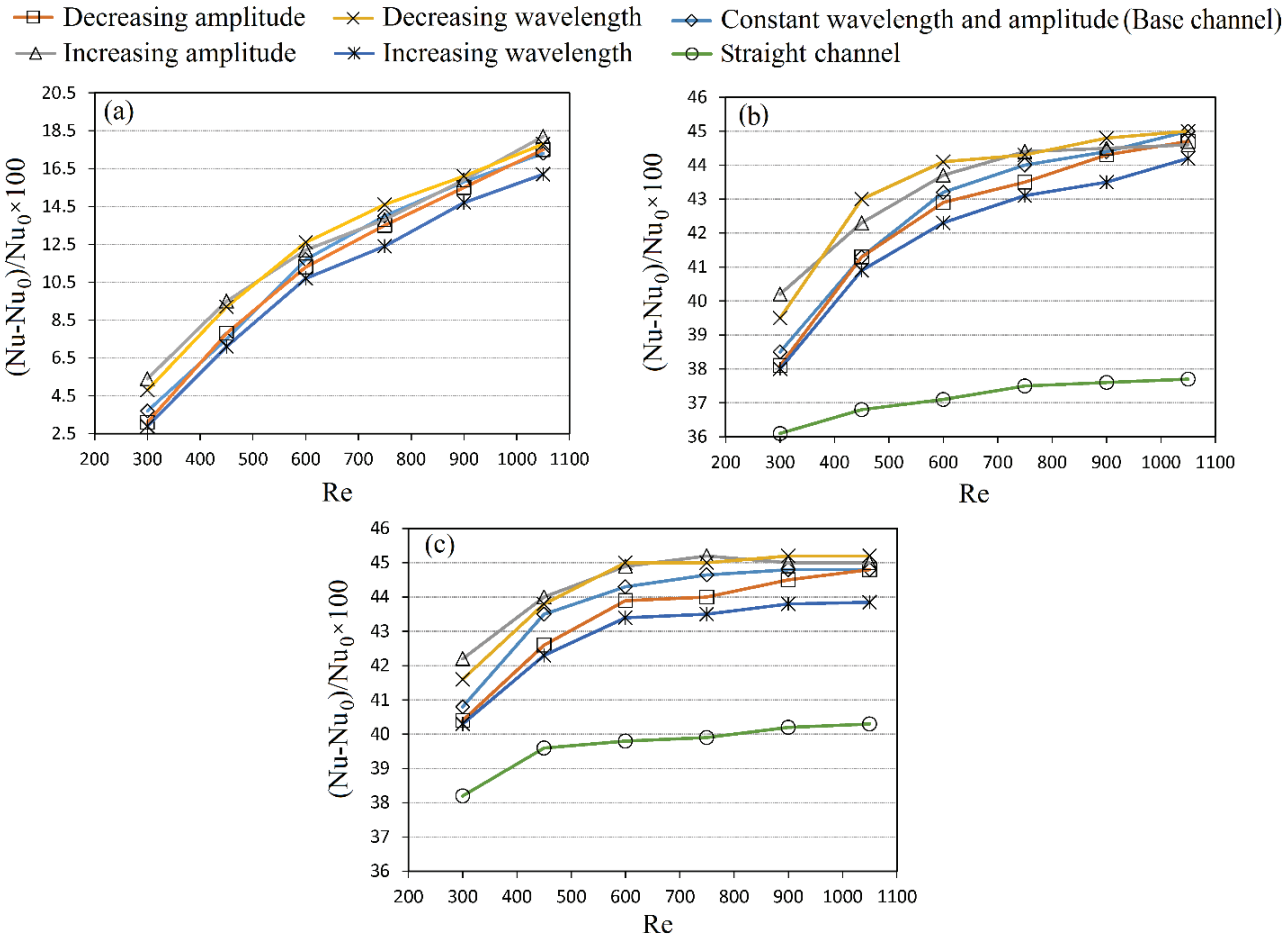

Figure 10. Variation of relative Nusselt number for (a) one-, (b) two- and (c) three-layer microchannels for the straight and wavy channels at different Reynolds numbers.

the channel layer increases from one to two is more remarkable than the channel layer increases from two to three. To justify this, one could refer to figure 8 that represent temperature contours at specified values of Reynolds number and distance from the channel inlet for one-, two- and three-layer base channel. This figure shows that an increase in the number of layers leads to the lower temperature difference between the wall and fluid temperatures especially for the upper layers of the microchannels. Since the Nusselt number has an inverse relationship with the temperature difference between the wall and fluid mean temperatures (see equations (3) and (4)), one could deduce that an increase in the number of the channel layers results in the increase in Nusselt number. Figure 8 also shows that as the number of layers increase from one to two, the difference between the wall and fluid temperatures becomes higher than that the number of layer increases from two to three. This confirms that as the number of layers increases from one to two, the increase in Nusselt number is more significant than that the number of layers increase from two to three.

To explain the effect of change in the number of layers on the fluid temperature rise, figure 11 presents mass average fluid temperature at the distance of 12000 μm from the channel inlet for the one-, two- and three-layer channels. This figure is provided for the base channels at Reynolds number of R_e=600. Exploring this figure reveals that the increase in the channel layer causes the fluid mean temperature to decrease. Figure 11 also shows the decrease in the fluid temperature is higher as the channel layers increase from one to two than that the channel layers increase from two to three.

Figure 8 reveals that for one-, two- and three-layer wavy channels, the highest relative Nusselt number corresponds to the decreasing wavelength and increasing amplitude cases. This due to the fact that for the decreasing wavelength channels, a higher mixing for the fluid could be attained than the other wavy channels. For the increasing amplitude channels, higher mixing as well as the increase in the contact surface area between the channel and fluid are the main causes for the increase in the Nusselt number. Referring to figure 8, one could see that the maximum relative Nusselt numbers for one-, two- and three-layer wavy channels are found to be 18.2%, 45% and 45.2%, respectively. Referring to figure 8, one could observe that for

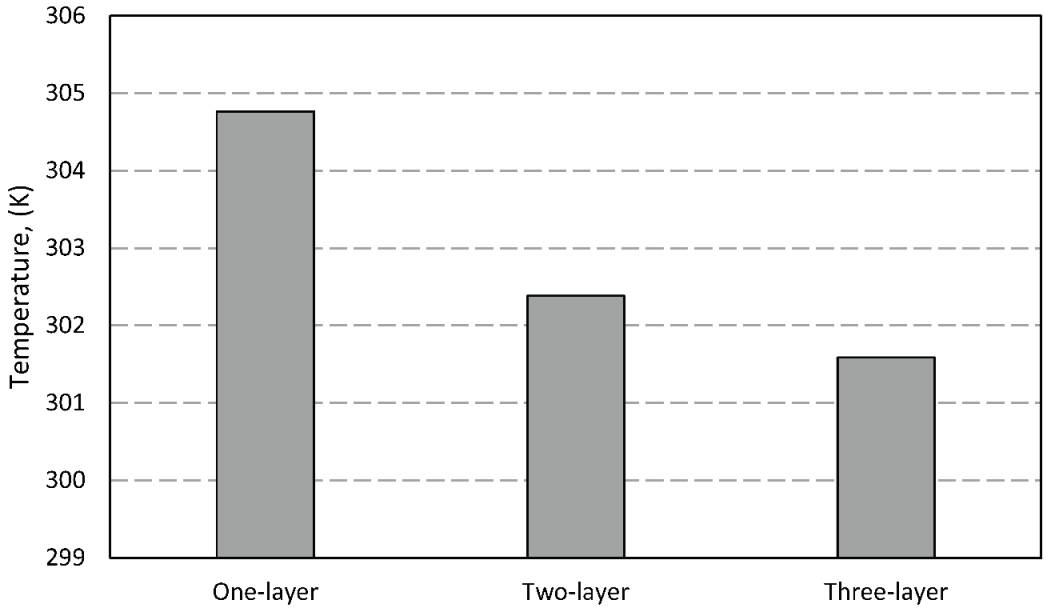

Figure 11. Average fluid temperature at the distance of 12000 μm from the channel inlet for the base channel at Reynolds number of R_e=600.

one-, two- and three-layer wavy channels, the increasing wavelength cases yield the lower relative Nusselt number as these cases result in a lower mixing for the fluid and also lower surface area than the other wavy channels.

Figure 8 shows that, as expected, an increase in the Reynolds number results in the increase in the relative Nusselt number for the considered channels. This figure reveals that the increase in the relative Nusselt number as the Reynolds number increases from R_e=300 to R_e=600 is remarkable than the Reynolds number increases from R_e=600 to R_e=1050. To explain this, temperature contours at the distance of 12000 μm from the channel inlet for the base channel at Retynolds numbers of R_e=300, 600 and 900 for the one-, two- and three-layer channels are shown in figures 12 to 14. Referring to these figures, one could realize that as the Reynolds number increases from R_e=300 to R_e=600, the decrease in the temperature of the solid portion of the domain is higher than that the Reynolds number increases from R_e=600 to R_e=900. These figures also represent that temperature distributions within the solid part at Reynolds numbers of R_e=600 and R_e=900 are closer to each other than those at Reynolds numbers of R_e=300 and

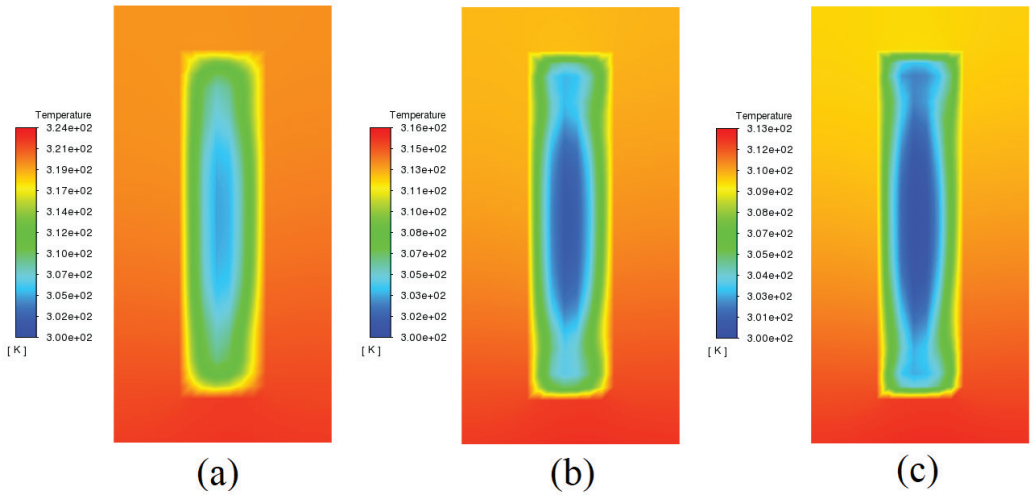

Figure 12. Temperature contours for the base channel at Reynolds number of (a) R_e=300, (b) R_e=600 and (c) R_e=900 for one-layer channel.

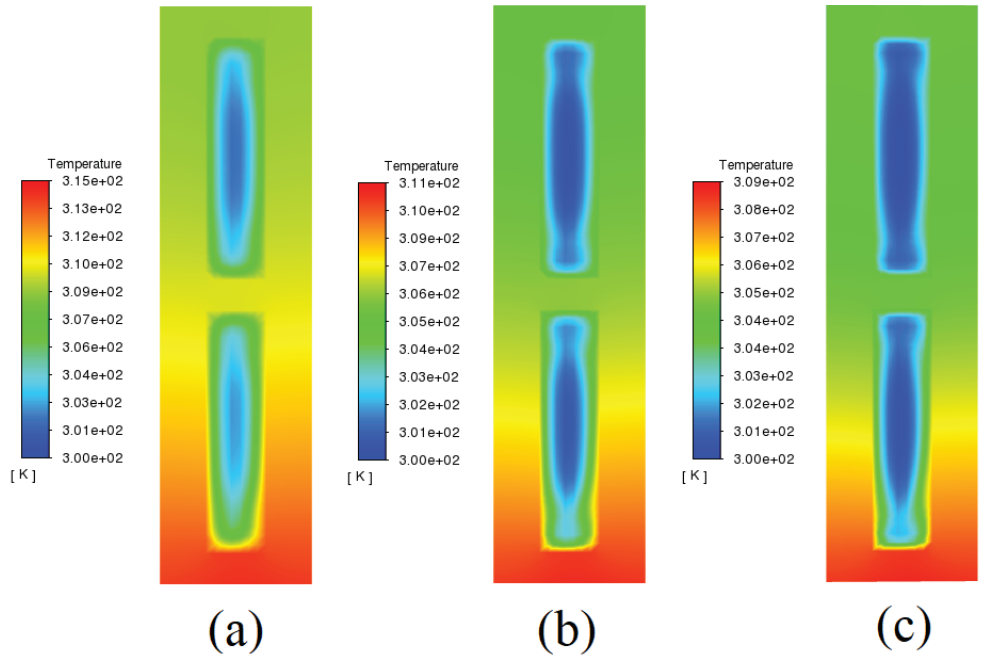

Figure 13. Temperature contours for the base channel at Reynolds number of (a) R_e=300, (b) R_e=600 and (c) R_e=900 for two-layer channel.

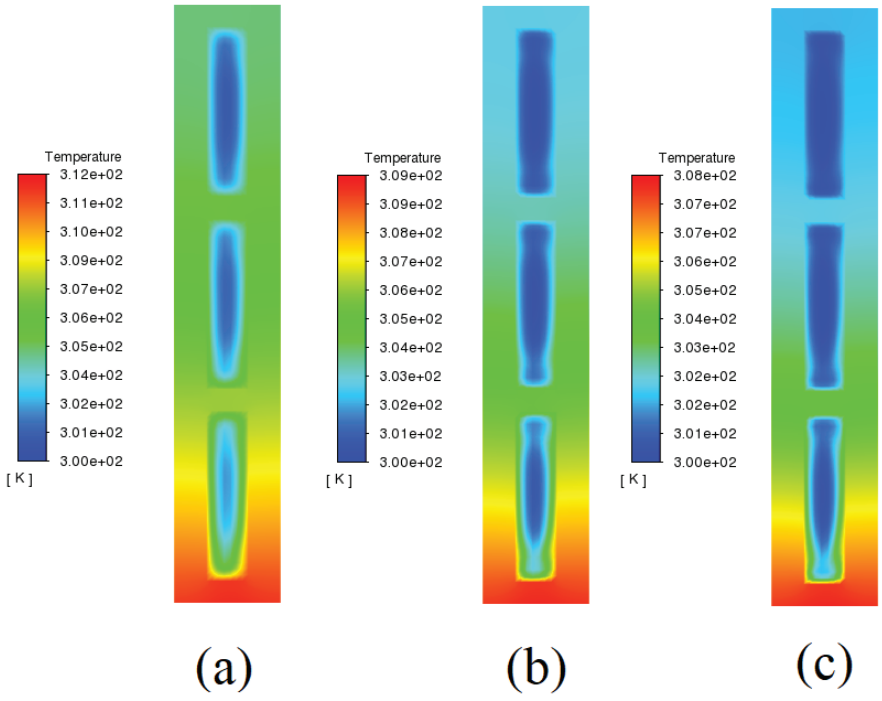

Figure 14. Temperature contours for the base channel at Reynolds number of (a) R_e=300, (b) R_e=600 and (c) R_e=900 for three-layer channel.

R_e=600. These imply that as the Reynolds number increases from R_e=300 to R_e=600, the channel capability in transferring the heat is higher than that the Reynolds number increases from R_e=600 to R_e=1050.

Effect on Overall Performance

Figures 15 shows variations of overall performance for one-, two- and three-layer channels at different values of Reynolds numbers. Overall performance is a significant

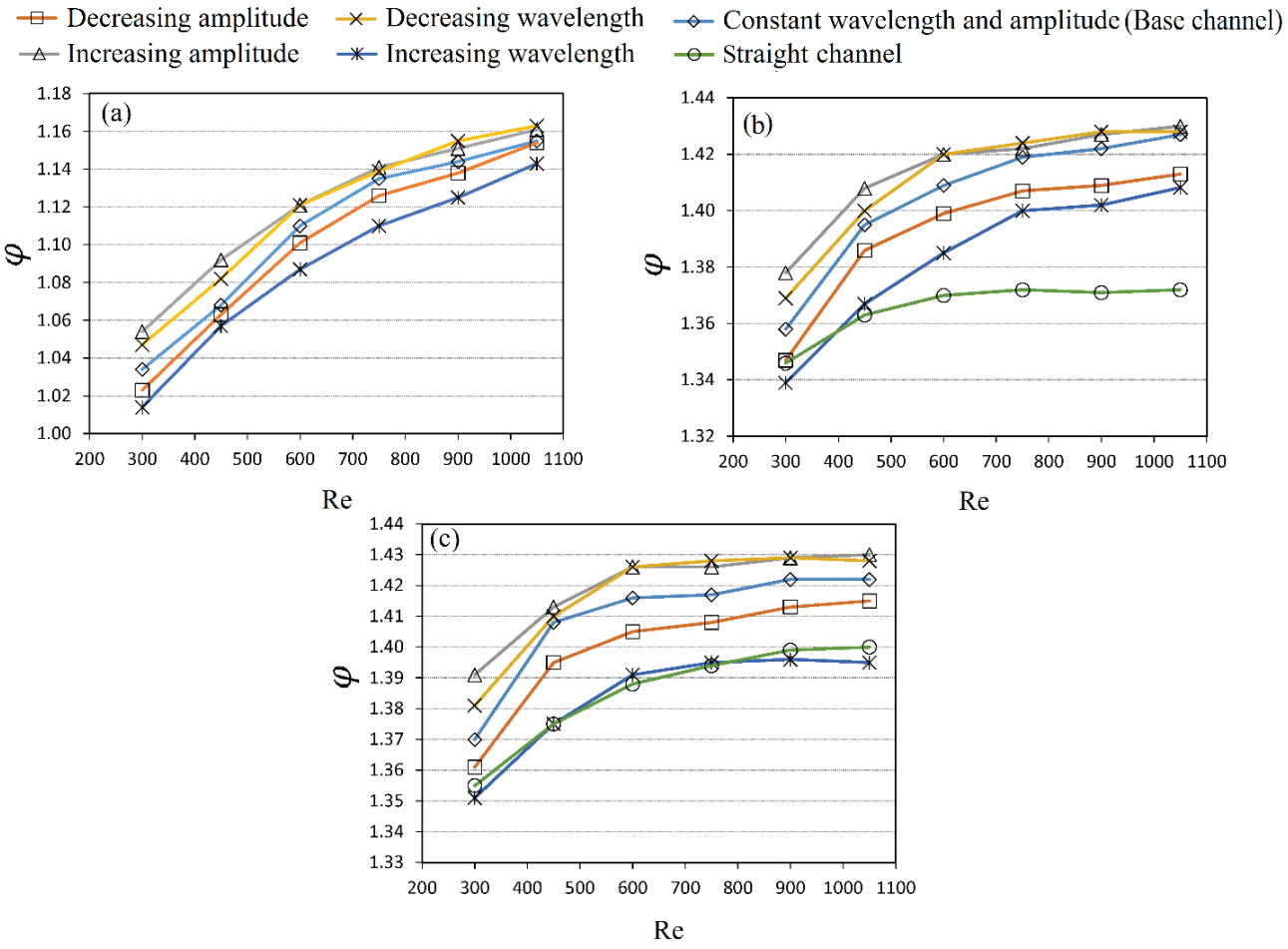

Figure 15. Variations of microchannel overall performance for (a) one-, (b) two- and (c) three-layer channel at different Reynolds numbers.

issue which must be taken into account in the design process of heat sink microchannel. As discussed in the work conducted by Kharati-Koopaee and Zare [32], overall performance compare somehow the capability of microchannel in transferring the heat with the penalty imposed by pressure loss.

Figure 15 shows that the overall performance increases with increasing the channel layers and overall performance enhancement is higher as the number of layers increases from one to two than that the number of layers increases from two to three. As presented in this figure, an increase in the Reynolds number causes the channel overall performance to increase. As presented in figure 15, for one-, two- and three-layer wavy channels, the lowest overall performances is associated to the case of increasing wavelength and the highest overall performance corresponds to increasing amplitude, although the case of decreasing wavelength has the same performance as the increasing amplitude at high Reynolds numbers (i.e., R_e=600 to 1050). Results also reveals that for one-, two- and three-layer channels, the change in channel structure form increasing wavelength to decreasing amplitude, and then to constant wavelength and amplitude, and finally to decreasing wavelength causes the channel overall performance to increase. Figure 15 shows that for one-, two- and three-layer wavy channels, the maximum overall performances are 1.16, 1.43 and 1.43, respectively.

CONCLUSION

In this work, the effect of change in the number of layers for the variable wavelength and amplitude wavy microchannels on the fluid flow and heat transfer phenomena at different Reynolds number are examined. To perform this, the changes in the friction factor and Nusselt number relative to those of the one-layer straight microchannel are studied. In the considered range of parameters, following results could be drawn:

- The relative friction factor increases as the channel layers increase due to increase in the fluid viscosity.
- The lowest and highest relative friction factors of the wavy microchannels correspond to the cases of

increasing amplitude and increasing wavelength, respectively. For one-, two- and three-layer microchannels, the relative friction factor increases as the channel configuration changes from decreasing wavelength to constant wavelength and amplitude, and finally to decreasing amplitude. For one-, two- and three-layer channels, the minimum relative friction factors are 0.1%, 3.7% and 4.7%, respectively.

- For the one-layer wavy microchannel, an increase in Reynolds number causes the relative friction factor to increase. This is due to the fact that for the one-layer microchannels, as Reynolds number increases, the impact of decrease in the fluid viscosity in decreasing the pressure loss is inferior to the effect of increase in the Reynolds number in increasing the pressure loss.
- For the two-layer channel, the relative friction factor decreases as the Reynolds number increases from R_e=300 to R_e=600 whereas the relative friction factor increases as the Reynolds number increases from R_e=600 to R_e=1050. The reason for that is due to superiority or inferiority of decrease in the fluid viscosity in reducing the pressure loss.
- For the three-layer channel, an increase in Reynolds number causes the relative friction factor to decrease. This is due to superiority of decrease in the fluid viscosity in decreasing the pressure loss than the increase in the Reynolds number in increasing the pressure loss.
- The relative Nusselt number increases as the channel layer increases and this increase is remarkable as the number of layers increases from one to two than the number of layers increases from two to three.
- For one-, two- and three-layer wavy channels, the highest relative Nusselt number corresponds to the decreasing wavelength and increasing amplitude cases and the lowest relative Nusselt number corresponds to the increasing wavelength case. Results also reveal that an increase in the Reynolds number results in the increase in the relative Nusselt number and this increase is remarkable as the Reynolds number increases from R_e=300 to R_e=600 than that the Reynolds number increases from R_e=600 to R_e=1050. The maximum relative Nusselt numbers for one-, two- and three-layer wavy channels are found to be 18.2%, 45% and 45.2%, respectively.
- The overall performance enhances with increasing the channel layers and overall performance enhancement is higher as the number of layers increases from one to two than that the number of layers increases from two to three. Results also show that an increase in the Reynolds number results in the in the increase in the channel overall performance. Numerical findings indicate that the lowest overall performances is associated to the case of increasing wavelength and the highest overall performance corresponds to increasing amplitude case. It is also shown that for one-, two- and three-layer channels, the change in the channel configuration from increasing wavelength to decreasing amplitude, and then to constant wavelength and amplitude, and finally to decreasing wavelength causes the channel overall performance to increase. For one-, two- and three-layer wavy channels, the maximum overall performance are 1.16, 1.43 and 1.43, respectively.

NOMENCLATURE

A	Wave amplitude
c_p	Specific heat, J/ kgK
D_h	Hydraulic diameter, m
f	Friction factor
h_m	Average heat transfer coefficient
k	Thermal conductivity, W / m K
Nu	Nusselt number
p	Pressure, N/m^2
P_w	Wetted perimeter, m
q''	Heat flux, W/m^2
R_e	Reynolds number
R_{ecr}	Critical Reynolds number
S	Area, m^2
T	Temperature, K
T_m	Mass average of fluid, K
T_w	Average wall temperature, K
U	Fluid velocity, m/s
u_i	Fluid velocity components, m/s
x_i	Spatial direction

Greek symbols

ρ	Density, kg/m^3
λ	Wavelenght, m
μ	Viscosity, Ns/m^2
φ	Overall performance

Subscripts

f	Refers to fluid
s	Refers to solid
0	Refers to one-layer straight channel
in	Refers to inlet property

AUTHORSHIP CONTRIBUTIONS

Authors equally contributed to this work.

DATA AVAILABILITY STATEMENT

The authors confirm that the data that supports the findings of this study are available within the article. Raw data that support the finding of this study are available from the corresponding author, upon reasonable request.

CONFLICT OF INTEREST

The author declared no potential conflicts of interest with respect to the research, authorship, and/or publication of this article.

ETHICS

There are no ethical issues with the publication of this manuscript.

REFERENCES

[1] Laidoudi H, Ameur H. Natural convection between hot and cold cylinders in enclosed space filled with wopper-water nanofluid. J Therm Engineer 2022;8:606−618. [CrossRef]

[2] Jang SP, Choi S. Cooling performance of a microchannel heat sink with nanofluids. Appl Therm Engineer 2006;26:2457−2463. [CrossRef]

[3] Zahmatkesh I, Shandiz MRH. Optimum constituents for MHD heat transfer of nanofluids within porous cavities. J Therm Anal Calorim 2019;138:1669−1681. [CrossRef]

[4] Dash B, Nanda J, Rout SK. The role of microchannel geometry selection on heat transfer enhancement in heat sinks: A review. Heat Transf 2022;51:1406−1424. [CrossRef]

[5] Rout SK, Hussein AK, Mohanty CP. Multi-objective optimization of a three-dimensional internally finned tube based on Response Surface Methodology (RSM). J Therm Engineer 2015;1:131−142. [CrossRef]

[6] Mohammed HA, Gunnasegaran P, Shuaib NH. Numerical simulation of heat transfer enhancement in wavy microchannel heat sink. Int Comm Heat Mass Transf 2011;38:63−68. [CrossRef]

[7] Liu GJ, Liu Y, Sunden B, Zhang W. Comparative study of thermal performance of longitudinal and transversal-wavy microchannel heat sinks for electronic cooling. J Electron Packag 2013;135:021008. [CrossRef]

[8] Solehati N, Bae J, Sasmito AP. Numerical investigation of mixing performance in microchannel T-junction with wavy structure. Comput Fluids 2014;96:10−19. [CrossRef]

[9] Rostami J, Abbassi A. Conjugate heat transfer in a wavy microchannel using nanofluid by two-phase Eulerian-Lagrangian method. Adv Powder Technol 2016;27:9−18. [CrossRef]

[10] Bazdar H, Toghraie D, Pourfattah F, Akbari OA, Nguyen HM, Asadi A. Numerical investigation of turbulent flow and heat transfer of nanofluid inside a wavy microchannel with different wavelengths. J Therm Anal Calorim 2020;139:2365−2380. [CrossRef]

[11] Eltaweel A, Baobeid A, Tompkins B, Hassan I. Numerical investigation of heat transfer characteristics of a novel wavy-tapered microchannel heat sink. In: Proceedings of ASME 14th Int. Conf. on Nanochannels, Microchannels, and Minichannels; 2016. [CrossRef]

[12] Gong L, Lu H, Li H, Xu M. Parametric numerical study of the flow and heat transfer in a dimpled wavy microchannel. Heat Transf Res 2016;47:105−118. [CrossRef]

[13] Lin L, Zhao J, Lu G, Wang XD, Yan WM. Heat transfer enhancement in microchannel heat sink by wavy channel with changing wavelength/amplitude. Int J Therm Sci 2017;118:423−434. [CrossRef]

[14] Kumar VR, Balasubramanian K, Kumar KK, Tiwari N, Bhatia K. Numerical investigation of fluid flow and heat transfer characteristics in novel circular wavy microchannel. Proc Inst Mech Engineer Part E J Process Mech Eng 2019;233:954−966. [CrossRef]

[15] Zhu JF, Li XY, Wang SL, Yang YR. Performance comparison of wavy microchannel heat sinks with wavy bottom rib and side rib designs. Int J Therm Sci 2019;146:106068. [CrossRef]

[16] Chong SH, Ooi KT, Wong TN. Optimisation of single and double layer counter flow microchannel heat sinks. Appl Therm Engineer 2002;22:1569−1585. [CrossRef]

[17] Shao B, Wang L, Cheng H, Li J. Optimization and numerical simulation of multi-layer microchannel heat sink. Procedia Engineer 2012;31:928−933. [CrossRef]

[18] Lin L, Chen YY, Zhang XX, Wang XD. Optimization of geometry and flow rate distribution for double-layer microchannel heat sink. Int J Therm Sci 2014;78:158−168. [CrossRef]

[19] Xu S, Wu Y, Cai Q, Yang L, Li Y. Optimization of the thermal performance of multi-layer silicon microchannel heat sinks. Therm Sci 2016;20:2001−2013. [CrossRef]

[20] Zhou F, Zhou W, Qiu V, Yu W, Chu X. Investigation of fluid flow and heat transfer characteristics of parallel flow double-layer microchannel heat exchanger. Appl Therm Engineer 2018;137:616−631. [CrossRef]

[21] Effat MB, AbdelKarim MS, Hassan O, Abdelgawad M. Numerical investigations of the effect of flow arrangement and number of layers on the performance of multi-layer microchannel heat sinks. In: Proceedings of ASME Int. Mechanical Engineering Congress & Exposition; 2015. [CrossRef]

[22] Wong KC, Ang ML. Thermal hydraulic performance of a double-layer microchannel heat sink with channel contraction. Int Comm Heat Mass Transf 2017;81:269−275. [CrossRef]

[23] Kumar A, Nath S, Bhanja D. Effect of nanofluid on thermo hydraulic performance of double layer tapered microchannel heat sink used for electronic chip cooling. Numer Heat Transf Part A 2018;73:429−445. [CrossRef]

[24] Shen H, Zhang Y, Yan H. Convective heat transfer of parallel-flow and counter-flow double-layer microchannel heat sinks in staggered arrangement. In: Proceedings of ASME Int. Mechanical Engineering Congress & Exposition; 2017. [CrossRef]

[25] Khodabandeh E, Rozati SA, Joshaghani M, Akbari OA, Akbari S, Toghraie D. Thermal performance improvement in water nanofluid/GNP-SDBS in

novel design of double-layer microchannel heat sink with sinusoidal cavities and rectangular ribs. J Therm Anal Calorim 2019;136:1333−1345. [CrossRef]
[26] Shen H, Xie G, Wang CC. Heat transfer and thermodynamic analysis by introducing multiple alternation structure into double-layer microchannel heat sinks. Int J Therm Sci 2019;145:105975. [CrossRef]
[27] Shen H, Xie G, Wang CC. The numerical simulation with staggered alternation locations and multiflow directions on the thermal performance of double-layer microchannel heat sinks. Appl Therm Engineer 2019;163:114332. [CrossRef]
[28] Xie G, Chen Z, Sunden B, Zhang W. Numerical predictions of the flow and thermal performance of water-cooled single-layer and double-layer wavy microchannel heat sinks. Numer Heat Transf 2013;63:201−225. [CrossRef]
[29] Xie G, Chen Z, Sunden B, Zhang W. Comparative study of the flow and thermal performance of liquid-cooling parallel-flow and counter-flow double-layer wavy microchannel heat sinks. Numer Heat Transf Part A 2013;64:30−55. [CrossRef]
[30] Shen H, Zhang Y, Wang CC, Xie G. Comparative study for convective heat transfer of counter-flow wavy double-layer microchannel heat sinks in staggered arrangement. Appl Therm Eng 2018;137:228−237. [CrossRef]
[31] Wang SL, Chen LY, Zhang BX, Yang YR, Wang XD. A new design of double-layered microchannel heat sinks with wavy microchannels and porous-ribs. J Therm Anal Calorim 2020;141:547−558. [CrossRef]
[32] Kharati-Koopaee M, Zare M. Effect of aligned and offset roughness patterns on the fluid flow and heat transfer within microchannels consist of sinusoidal structured roughness. Int J Therm Sci 2015;90:9−23. [CrossRef]
[33] Sui Y, Lee PS, Teo CJ. An experimental study of flow friction and heat transfer in wavy microchannels with rectangular cross section. Int J Therm Sci 2011;50:2473−2482. [CrossRef]